We are IntechOpen,
the world's leading publisher of
Open Access books
Built by scientists, for scientists

6,900
Open access books available

186,000
International authors and editors

200M
Downloads

154
Countries delivered to

Our authors are among the

TOP 1%
most cited scientists

12.2%
Contributors from top 500 universities

BOOK CITATION INDEX
CLARIVATE ANALYTICS
INDEXED

WEB OF SCIENCE™

Selection of our books indexed in the Book Citation Index
in Web of Science™ Core Collection (BKCI)

Interested in publishing with us?
Contact book.department@intechopen.com

Numbers displayed above are based on latest data collected.
For more information visit www.intechopen.com

Automatic Mapping of the Lava Flows at Piton de la Fournaise Volcano, by Combining Thermal Data in Near and Visible Infrared

Z. Servadio[1,2], N. Villeneuve[1] and P. Bachèlery[3,4]
[1]Laboratoire Géosciences Réunion, Université de la Réunion,
Institut de Physique du Globe de Paris, CNRS, UMR 7154,
Géologie des Systèmes Volcaniques, Saint Denis
[2]Institut de Recherche pour le Développement, US 140,
BP172, 97492 Sainte-Clotilde Cedex
[3]Clermont Université, Université Blaise Pascal,
Laboratoire Magmas et Volcans, CNRS, UMR 6524,
Observatoire de Physique du Globe de Clermont-Ferrand,
BP 10448, F-63000 Clermont-Ferrand
[4]IRD, R 163, LMV, F-63038 Clermont-Ferrand
France

1. Introduction

Knowing the eruptive history of a volcano is an essential key to the understanding of its functioning, and therefore of the evolution of the character of dangerousness of its eruptions. For an essentially effusive basaltic volcano such as the Piton de la Fournaise, the spatial and temporal distribution of lava flows allows to deduct numerous parameters of its activity, on a magmatic and a structural point of view. Satellite imaging brings more advantages than the methods used in aerial pictures studies, especially by supplying bigger temporal and spectral series. The revisiting of satellites over a region can allow the generation of dynamic mappings of the implementation of the lava flow, and also bring information on the phenomenology of the eruptions: Surface, volume, flow, spatial distribution…

Furthermore, satellite images have the advantage of supplying data that grant a global visualization of the study area, and information on not easily accessible areas. The interpretation of these satellite data enables obtaining information on the surfaces and volumes of the lava field flows, but also on its nature and behavior. In a tropical environment such as La Reunion, where the climatological context presents a strong cloudiness, a satellite revisit is statistically necessary.

The optical satellite images have already been successfully used to realize mappings of lava flows. For example, in Nevado Subancaya in Peru (Legelay-Padovanie et al., 1997) or in Etna in Italy (Honda et al.,2002), the combination of spectral and morphological properties helped to elaborate surface lava flows mappings and also allowed to individualize the main

structures. Lu et al. (2004) propose an association of OPTICAL and RADAR imaging in order to define more accurate outlines for the lava flows. In the later example, the downstream part of the lava flow presenting vegetation, the discrimination was realized by the infrared. The upstream part being a heavily snow covered zone, RADAR images properties become a precious source of information. Thanks to the use of LIDAR (Airborne Light Intensity Detection and Ranging) on volcanoes, Digital Ground Models of very high-resolution can be generated and various retro-reflecting properties of the lava's different textures can be studied (Favalli et al., 2009) .The comparison of the different DGM produced at different dates allow Favalli et al. (2009) to obtain mappings of the thickness and outlines of the lava flow.

The use of thermal satellite imaging to characterize the relative chronology of the implementation of lava flows was the aim of Kahle et al. (1998)'s work. Abrams et al. (1991), used it in association with optical satellite imaging to realize a chronological mapping of the lava flows in Hawaii. Other authors have realized mappings of lava flow's temperature (Hirn et al., 2005) and implementation maps by using a thermal camera (Harris et al., 2007; James et al., 2007; Lombardo et al., 2009).

At the Piton de la Fournaise, the first research that used photogrammetry to realize mappings of the outlines and thickness of lava flows took place on lava flows dated back to 1972 and 1976 (Lénat, 1987). Bonneville et al. (1989) mapped the main geological units by using SPOT1 images. After which, Despinoy (2000) realized a mapping of the lava flows above Les Grandes Pentes using a CASI hyperspectral sensor. Villeneuve (2000) realized outlines, volume calculations and a chronological follow up of the implementation thanks to stereophotogrammetry and the use of DGPS (Digital Global Positioning System). Lénat et al. (2001) associated RADAR and SPOT images to map the field of lava of the Enclos Fouqué's caldera. Recently, De Michele et Briole (2007) used a technic of correlation of images to extract lava flows which implemented between two series of aerial pictures. The study of the incoherencies in the interferograms helped realize a dynamic follow up and a mapping of the lava flows (Tinard, 2007 ; Froger et al., 2007 ; Froger et al., in press).

The aim of this article is to propose an original approach by combining thermal images with ones acquired in the visible and near infrared in order to extract independent outlines for each lava flow. The extraction is therefore independent of the operator's subjectivity. Only one automatic extraction is possible when associating thermal and optical images for the implementation of a lava flow. An automatic extraction of the outlines of lava flow is realized and then compared to a mapping of references realized by photo-interpretation. We can therefore estimate the precision of the automatic extraction.

2. Context

The Piton de la Fournaise (Reunion Island, Indian Ocean) is a basaltic volcano whose functioning is connected to the activity of a hot spot (Courtillot et al. 1986). The eruptions take place inside the Enclos Fouqué's caldera and have contributed to the creation of a volcanic cone whose summit is occupied by two craters: the Bory on the east side and the Dolomieu on the west side (figure 1).

During the past three decades and besides the 1986 and 1998 exceptions, the lava flows have been taking place inside de Enclos Fouqué's caldera (figure 1 and 4). They are mainly fed by
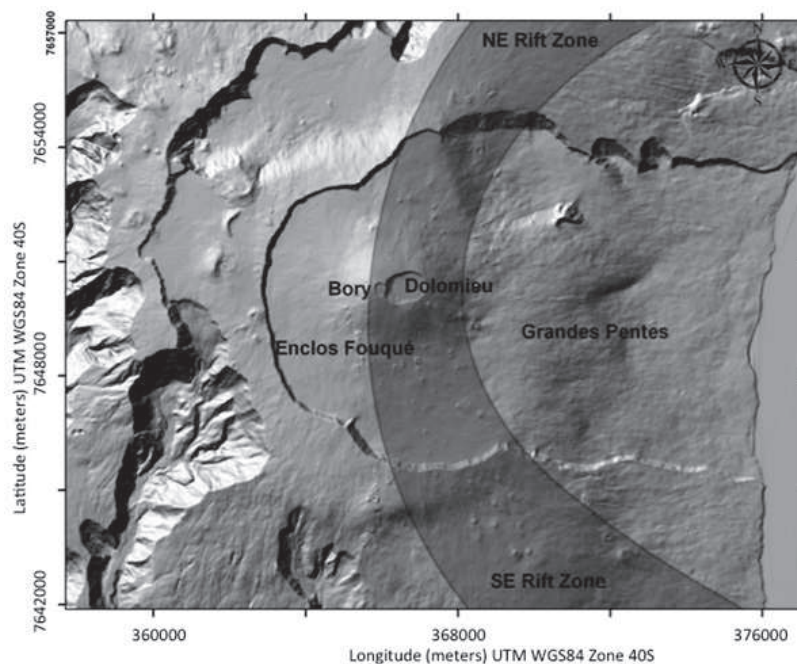
Fig. 1. Major morphological figures of the Piton de la Fournaise, the grey area is the rift zone defined by Bachèlery (1981).

intrusions situated along the rift zones (Bachèlery, 1981). The intrusions are interconnected at the same level as the central cone. Eruptions are of three kinds: summit zone eruptions, proximal eruptions, and distal eruptions (Peltier et al. 2009). It is clear that in the recent history of the Piton de La Fournaise, summit zone eruptions are the most frequent (Villeneuve et Bachèlery, 2006; Peltier et al., 2009). Most of these eruptions take place according to leveled cracks that progressively migrate by furthering from the central cone (Bachèlery, 1981).

Degassing at the event during eruptions can generate lava fountains which cause pyroclastic deposits and cones of several meters high. Two morphologies of lava flow are observed at Piton de la Fournaise: 'a'a type lava flows and pahoehoe type lava flows.

The occidental part of the Enclos Fouqué is largely recovered by a vast field of lava that Lénat et al. 2001 name the CLEF (Champ de Lave de l'Enclos Fouqué). This field of lava, essentially formed by a pahoehoe lava type flow, may have been constituted from slow emissions from the volcano's summit zone, between 1750 and 1794.

At the Piton de la Fournaise, the flow of lava emitted by eruptive cracks represent long (several meters to several kilometers), thin, (about ten meters), shallow (one meter in the slopes to 5 meters in flat zones (Letourneur et al., 2008)) lava flows, which shows the poor viscosity of the emitted magma. The juxtaposition of several individual flows during a same phase will contribute to the constitution of fields of lava, and particularly for long time eruptions (more than one month). In this case, in regards to the initial lava flow, the new income contributes essentially to the thickening and widening of the lava field flow. In this case, the lava field will be considered here as a same unit.

The spectral properties of the lava flows differ according to the type of the surface (mainly 'a'a type at Piton de la Fournaise), but also according to the age, either because of a chemical

transformation of the rock on the surface, or because of the implantation (always very fast in Reunion Island) of a vegetation cover (lichen, moss, shrub…). Lava flows which implementations were separated by several years can therefore be distinguished by their spectral properties. For the summit zone of the volcano, all the more in the Dolomieu crater, where the rocks are superimposed with only a few years or a few months of interval, the spectral properties of the diverse lava flows can then be very similar.

The oldest known eruption at the Piton de la Fournaise dates back to 1644. About 200 events have been counted since that date thanks to archives, 95% of them took place in the caldera (Lacroix, 1936; Stieltjes et al., 1989; Peltier et al. 2009). Never the less, this database is incomplete, particularly in the case of short time and low scale eruptions, before 1980. The mean average magma emission at Piton de la Fournaise estimated over a century, is 0,01 km^3.an^{-1} (Lénat et Bachèlery, 1987), or 0.3 m^3.s^{-1}. The debit estimations show a temporal estimation. For example, Stieltjes et al. (1989), calculate a mean debit of 0.3 m^3.s^{-1} over 54 years (1931-1985), but obtain 0.78 m^3.s^{-1} for a period of 25 years (1960-1985). These variations are partly due to the existence of long periods of inactivity. For example, no eruption took place during 1992 and 1998; witch is to say 6 years of inactivity. Also, another inactivity as long was observed between 1966 and 1972 (Villeneuve, 2000). Peltier et al. (2009) illustrate these debits variation and show a more important activity since 1998. Between January 1990 and January 2010, 61 eruptions have been registered with a total volume of emitted lava estimated at 473 Mm^3 (figure 2), and 33 eruptions between 1998 and 2010, with a total volume of emitted lava of 313 Mm^3 (Peltier et al. 2009, OVPF 2009; 2010). From these observations, we have calculated a mean debit estimated between 0.45 m^3.s^{-1} and de 0.82 m^3.s^{-1}, from 1980 to 2010. These estimations are superior to those obtained by Stieltjes et al. (1989), on former periods.
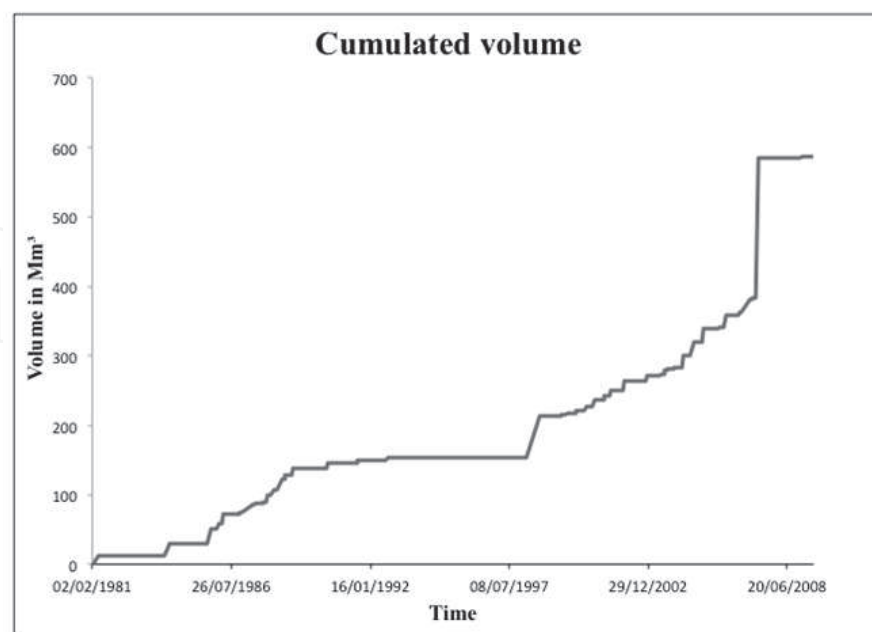

Fig. 2. Estimation of the cumulative volume of lava emitted from 1980 to 2010 by the Piton de la Fournaise.

3. Method

The originality of this research states in the use of thermal data as an analyze mask. In spite of its low spatial resolution (90m), thermal data brings essential information in our automatic mapping method. It allows determining with certitude the zone where the newly implemented lava flow is localized. The automatic extraction of the outline can be realized in this analyze mask. Also, its utilization enables treating the lava flows separately from one another because for one thermal image, only one lava flow is associated in this methodology. This is particularly adapted in the case of the constitution of a lava field flow.

3.1 Optical and thermal data

The automatic extraction method has been realized by the combination of thermal and optical data. SPOT and ASTER data have been used. SPOT data have **a** wavelength from the visible to mid infrared, and a spatial resolution from 2,5 to 20 meters. ASTER data have a spectrum from visible to thermal infrared and a spatial resolution that varies from 15m (VNIR) to 90m (TIR).

The ASTER TIR thermal data have to be acquired at the end of the eruption or very little time afterwards, in order for the thermal anomaly to be clearly visible on the entire zone. The maximum post eruption delay of acquisition is variable and depends on the thickness of the lava flow and therefore on its speed of cooling. In most of the cases, it is less than a month. ASTER VNIR and SPOT data can be acquired long after the lava flow's implementation. The principal is not having a new lava flow implementing on the same zone. The recent lava flows present low reflectances between the visible and mid infrared wavelength. The basalt spectrum, in the visible and short wavelength of the infrared (0.4-2.4 µm), is dominated by the presence of iron, which, at different levels of crescent oxidation, increases the reflectance (Despinoy, 2000). In the same way, the presence of lichen that grows on the lava flow increases the reflectance. In near and medium infrared, the presence of chlorophyll in the vegetation induces a strong signal (Kahle et al. 1995), permitting to discriminate precise outlines in zones with vegetation cover, especially near the Grandes Pentes area as for the Piton de la Fournaise.

The KALIDEOS project from the CNES (Centre National d'Etudes Spatiales, and GEO Grid (AIST/METI), and the NASA, grant free satellite data in the case of a research program. The data used in this article are from SPOT data from the KALIDEOS program, and from the GEO Grid program for the ASTER (Advanced Spaceborne Thermal Emission and Reflection Radiometer) data. The climatological conditions must be optimal because the presence of clouds masks, deforms or reduces the thermal anomaly, which in a tropical zone and especially in the volcano's zone is frequent. Only seven ASTER TIR data (the ASTER satellite was released in orbit in December 1999), acquired at the end of the eruption don't present these types of issues, and have therefore been used for the treatments (Table 1 and figure 3). Optical data acquired after the eruption have been associated to the former images.

3.2 Error calculation and outlines precision of photo-interpretation

The precision of the outlines extracted by automatic method leans entirely on their comparison with a base of outlines realized from very high-resolution satellite data' photo interpretation, and aerial pictures from IGN. This base is considerate as a reference.
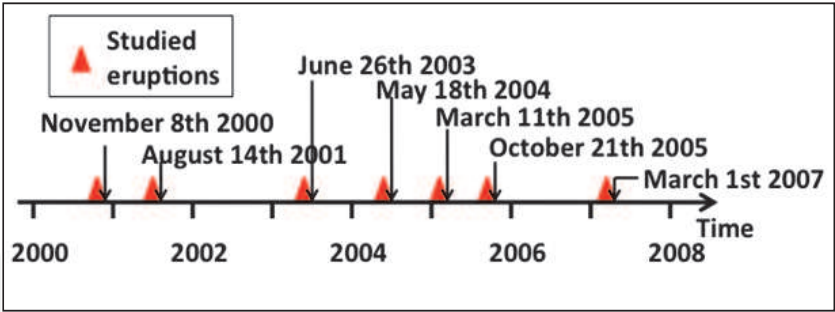
Fig. 3. Chronology of the acquisitions of the thermal data from the eruptions at the Piton de la Fournaise.

Eruption	ASTER TIR thermal Data		SPOT et ASTER optical data		
	Acquisition date (AAAAMMJJ)	Resolution	Acquisition date	Angle	Resolution
20070218	20070301	90m	20070314	R 19.1	10m
20051014	20051021	90m	20051222	R 25.9	10m
20050217	20050311	90m	20050217	6.7	15m
20040502	20040518	90m	20040518	-5.6	15m
20030530	20030626	90m	20031120	R 25.8	20m
20010611	20010814	90m	20010715-20011223	R 26.2 R 19.2	20m
20001012	20001108	90m	20001213	L 4.3	20m

Table 1. SPOT and ASTER data used for automatic treatments.

The outlines realized after photo interpretation, also known as reference, are not without errors. They contain errors linked to the operator's subjectivity and from the resolution of the data used to extract the outlines. One has to take into consideration these imprecisions before interpreting the results. This will be approached in the photo interpretation chapter, where outlines extracted by satellite data' photo interpretation are tested and compared on the base of those extracted from IGN's aerial pictures.

The method chosen lies on the constitution of an error matrix, because it permits to know the precision of all or part of the classification. It's expressed in percent or area.

3.2.1 Error matrix

The error matrix enables comparing two thermal maps. These matrixes are constructed according to a methodology developed by the Remote sensing Center of Canada (http://ccrs.nrcan.gc.ca/glossary/index_e.php?id=3124).

In our study case, an outline is compared to another that will be considered as reference (table 2).

In the matrix, numbers contained by cells correspond to areas. The total of the areas by column represent the total area of the class obtained by automatic classification. The total of the areas of each line corresponds to what has been correctly classified. The area values present in the diagonal correspond to the ones correctly classified. The other cells represent the areas which were classified wrong, either by omission, or by commission (table 2).

Areas (Km²)	Classification Data		
Reference Classification	Lava Flow	No Lava Flow	Σ
Lava Flow	Correctly classified Lava Flow	Omission Error	**Reference Lava Flow Area**
No Lava Flow	Commission Error	Correctly classified No Lava Flow	**Reference No Lava Flow Area**
Σ	**Automatic Lava Flow Area**	**Automatic No Lava Flow Area**	**Study Area**

Table 2. An error matrix for two classes
(http://ccrs.nrcan.gc.ca/glossary/index_e.php?id=3124 (modifiée)).

It is therefore possible to calculate a global precision (in percent) of the classification, which is to say the area of what has been classified correctly in regards to the total area of the zone that has been classified

$$Pg = \frac{\sum Well\ class\ area}{total\ area\ of\ the\ study} * 100$$

It is also interesting to look at the mean precision of each class of classification:

$$Pm = \frac{Pmi}{i}$$

The precision of each class is different. Some pixels can be attributed to classes that don't suit them, if the spectral properties are similar. The exactitude producer (table 2) bases itself on the area of the pixels correctly classified in regards to the area of the lava flow considered as reference. As for the exactitude user (table 2), it bases on the area of the pixel correctly classified in regard to the area of the lava flow obtained by extraction.

The exactitude producer of the "lava flow" class allows knowing the accuracy of the outline obtained by automatic extraction:

$$Pm\ (lava) = \frac{Well\ class\ area}{Real\ lava\ flow\ area} * 100$$

The mean distance separating outlines vectors is calculated from the area which was not correctly classified, divided by the smallest of the two compared lava flow outline's perimeter:

$$Error\ \beta = \frac{\sum Not\ correctly\ class\ area}{Perimeter} * 100$$

3.2.2 Photo interpretation

The « referenced » outlines have been realized on a period from 1980 to 2010, by vectorization on the base of IGN aerial data from 1997 and 2003. As for the eruptions post August 2003, the research was done on a base of SPOT THR, or SPOT 4 AND 5 satellite data (Figure 4). The vectorization of the lava flows by using aerial photos is one of the most precise (Paparoditis et al. 2006), but it is also one of the most binding to realize. It could ask for several worked days.
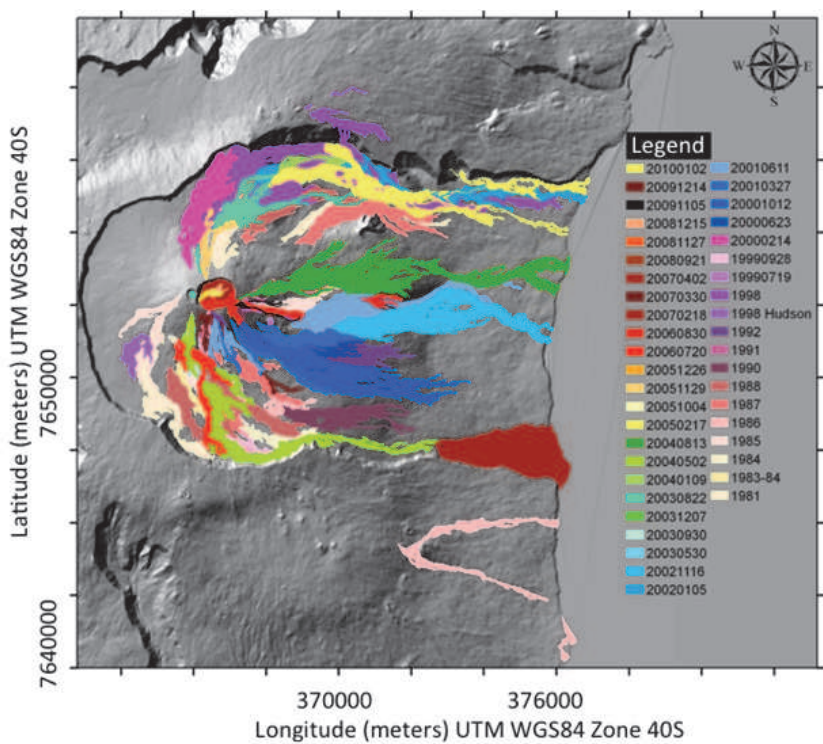

Fig. 4. Piton de la Fournaise lava flow cartography between 1980 and 2010 (Servadio et al. 2008 modified).

For the entire French territories, the temporal recurrence in the IGN's acquisitions is 5 years. It is a problem when dealing with superimposed lava flows. Satellite imaging is then a complementary tool because, even if the spatial resolution of SPOT data is lower (2,5m to 20m with optical SPOT data, or inferior or equal to 1 meter with aerial photos delivered by IGN for the BDORTHOs), the temporal resolution grants data between eruptions and defines outlines for the superimposed zones. Unfortunately, the resolution of the outlines is

then less precise. The SPOT satellite was put into function in 1986, the outline data base was completed by the mappings of the OVPF and the BRGM (Stieltjes et al., 1985 et 1989 ; Billard, 1974 ; Bussière, 1967 ; Mc Dougall, 1971).

Our methodology leans on different types of satellite data, it is important to know the influence of the spatial resolution on the extracted outlines. A comparison between the outlines obtained by photo-interpretation of different data and the referenced outlines is then done by using an error matrix and a mean distance between the outlines (table 3). According to the used satellite data, the awaited error on the outline is about the same size of the pixel (table 3). The classification's precision can tell that a mapping by satellite data' photo-interpretation is 85% more reliable for satellite data with a 10m to 20 m resolution, and 95% reliable for THR SPOT data (table 3). The other error due to the referenced outlines extraction can be the consequence of the operator's subjectivity. It presents an error from 2% to 5%. The same test was run from aerial photos, and the errors didn't exceed 2%.

3.2.3 Automatic process: TIR- VNIR method

The lava flows which implement in zones where spectral properties are different, such as a vegetation zone or a soil that presents high spectral reflectances, are the easiest to identify (figure 5).
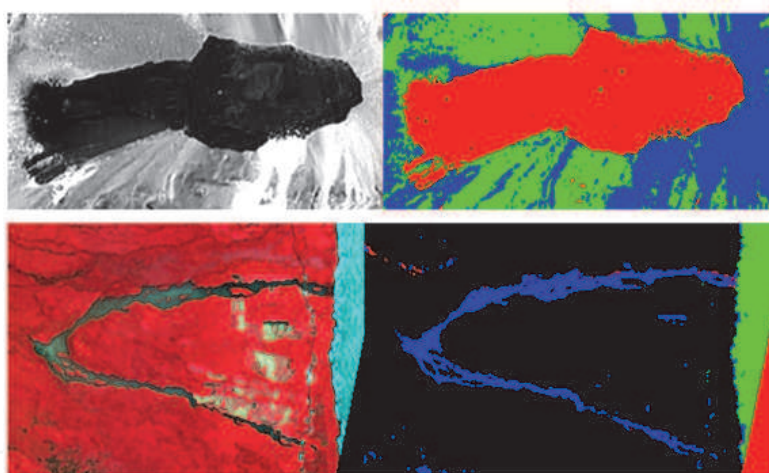

Fig. 5. Examples of automatic extraction of the lava flow outline when the reflectance of the substrate is very different from that of the lava. A and B: lava flow from the eruption of September 2009. C and D: lava flow from the eruption of 1986 off enclosures.

To automatically extract an outline, different methods can be used: classifications, threshold, or automatic detection of change (Inglada et al., 2003; Habib et al., 2007). The distance between the referenced outlines and the outlines automatically extracted is then proportional to the pixel's size, and the lava flow's classification precision is between 95% and 99%. On the other hand, lava flows which implement in low spectral reflectance zones, such as the central cone of the Piton de la Fournaise or the upperstream part of the Grandes Pentes, ask for more complex treatments. A data treatment methodology is then put together by using ENVI software (Figure 6). The visible data Principal Composant Analysis (PCA) is applied in order to maximize the data's anti-correlation. The thermal bands, near
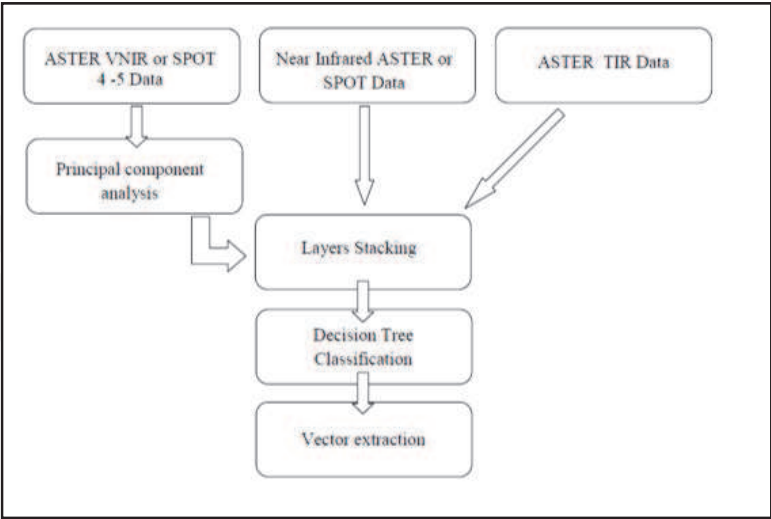
Fig. 6. TIR-VNIR Treatment sequences

infrared and the PCA are grouped in a multi-band data. A multi-level binary classification named decisional tree classification is then applied by using the following steps:

- By using thermal data, distinguish « hot » from « cold » zones.
- Extract and keep only « hot » zones.
- Discretization of the bare soil and covered vegetation zones by using the Near Infra-red band.
- Classify the pixels with low anti-correlation values.

The seven lava flows for which ASTER data were available (table 1) were tested. For half of them, the tested eruptions are on a weak slope zone, with a substrate composed of lava flows with similar spectral properties; the other half shows various substrates and slopes (figure 7).
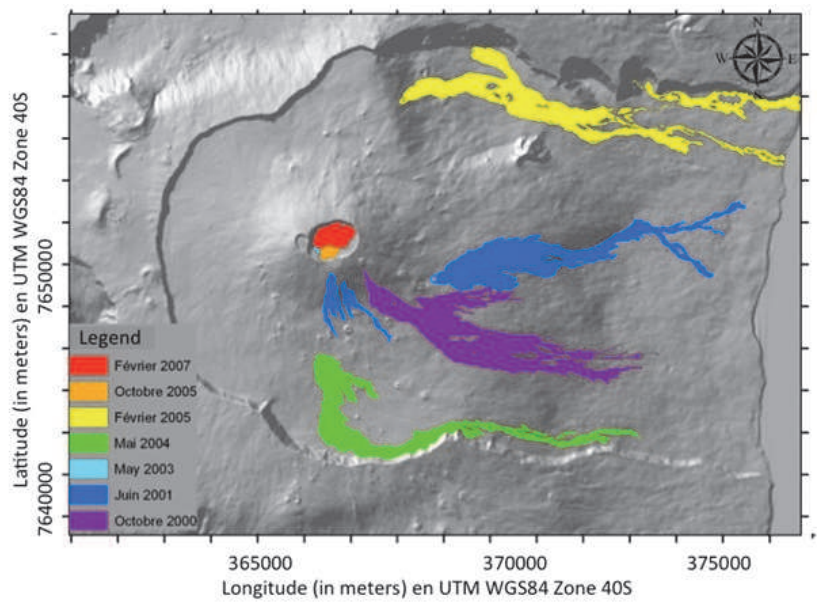

Fig. 7. Localization of the studied lava flows

Spot 4 20m

Aerial Pictures — 1991	Lava Flow class	No lava flow class	Producer's Accuracy
Lava flow	0.7632	0.0594	0.8226
No Lava flow	0.3848	3.0936	3.4784
User's accuracy	1.148	3.153	4.301
Global Accuracy		89.67%	
Mean Accuracy		90.86%	
Producer accuracy lava flow		92.78%	
Producer accuracy no lava flow		88.94%	
Mean distance between the outlines		30.5m	

20001012	Lava Flow class	No lava flow class	Producer's Accuracy
Lava flow	3.354	0.727	4.081
No Lava flow	1.273	9.796	11.069
User's accuracy	4.627	10.523	15.15
Global Accuracy		86.80%	
Mean Accuracy		85.34%	
Producer accuracy lava flow		82.18%	
Producer accuracy no lava flow		88.99%	
Mean distance between the outlines		38.86m	

Spot 5 10m

Global Accuracy — 1986	Lava Flow class	No lava flow class	Producer's Accuracy
Lava flow	1.017	0.165	1.182
No Lava flow	0.126	11.912	12.038
User's accuracy	1.143	12.077	13.22

ASTER VNIR 15m

Aerial Pictures — 20070402	Lava Flow class	No lava flow class	Producer's Accuracy
Lava flow	3.568	0.041	3.609
No Lava flow	0.141	1.738	1.879
User's accuracy	3.709	1.779	5.488
Global Accuracy		96.68 %	
Mean Accuracy		95.68%	
Producer accuracy lava flow		98.86%	
Producer accuracy no lava flow		92.49%	
Mean distance between the outlines		13.7m	

Spot 5 THR 5m

Aerial Pictures — 1998	Lava Flow class	No lava flow class	Producer's Accuracy
Lava flow	7.533	0.364	7.897
No Lava flow	1.327	23.636	24.963
User's accuracy	8.860	24	32.86
Global Accuracy		94.85%	
Mean Accuracy		95.04%	
Producer accuracy lava flow		95.09%	
Producer accuracy no lava flow		96.57 %	
Mean distance between the outlines		5m	

5m

20000214	Lava Flow class	No lava flow class	Producer's Accuracy
Lava flow	1.705	0.088	1.7893
No Lava flow	0.219	6.171	6.39
User's accuracy	1.924	6.259	8.183

Table 3. Continued

	Lava Flow class	No lava flow class	Producer's Accuracy
Global Accuracy	97.95%		
Mean Accuracy	92.5%		
Producer accuracy lava flow	86.04%		
Producer accuracy no lava flow	98.95%		
Mean distance between the outlines	10.7m		
20010611	Lava Flow class	No lava flow class	Producer's Accuracy
Lava flow	3.119	0.339	3.458
No Lava flow	0.412	13.22	13.632
User's accuracy	3.531	13.559	17.09
Global Accuracy	95.61%		
Mean Accuracy	93.59%		
Producer accuracy lava flow	90.20%		
Producer accuracy no lava flow	96.98%		
Mean distance between the outlines	8.9m		
20030530	Lava Flow class	No lava flow class	Producer's Accuracy
Lava flow	0.2536	0.0295	0.2831
No Lava flow	0.0908	0.4277	0.5185
User's accuracy	0.3444	0.4572	0.8016
Global Accuracy	84.90 %		
Mean Accuracy	86.03%		
Producer accuracy lava flow	89.58%		
Producer accuracy no lava flow	82.49%		
Mean distance between the outlines	11.7m		

	Lava Flow class	No lava flow class	Producer's Accuracy
Global Accuracy	96.25%		
Mean Accuracy	95.83 %		
Producer accuracy lava flow	95.09%		
Producer accuracy no lava flow	96.57 %		
Mean distance between the outlines	6.6m		
20010327	Lava Flow class	No lava flow class	Producer's Accuracy
Lava flow	2.510	0.105	2.615
No Lava flow	0.879	11.476	12.355
User's accuracy	3.389	11.581	14.97
Global Accuracy	93.43%		
Mean Accuracy	94.43%		
Producer accuracy lava flow	95.98%		
Producer accuracy no lava flow	92.89%		
Mean distance between the outlines	3.2m		
20020105	Lava Flow class	No lava flow class	Producer's Accuracy
Lava flow	2.581	0.169	2.750
No Lava flow	1.057	8.103	9.16
User's accuracy	3.638	8.272	11.91
Global Accuracy	89.71 %		
Mean Accuracy	91.16%		
Producer accuracy lava flow	93.85%		
Producer accuracy no lava flow	88.46 %		
Mean distance between the outlines	5.3m		

Table 3. Error matrices of outlines obtained by photo-interpretation, comparing those from the photo-interpretation of aerial photographs with those of the different types of satellite data.

The classification achieved, it is then possible to export the « lava flow » class as a vector that represents the outline of the lava flow (figure 8). The extraction is realized in less than an hour, once the data collected.
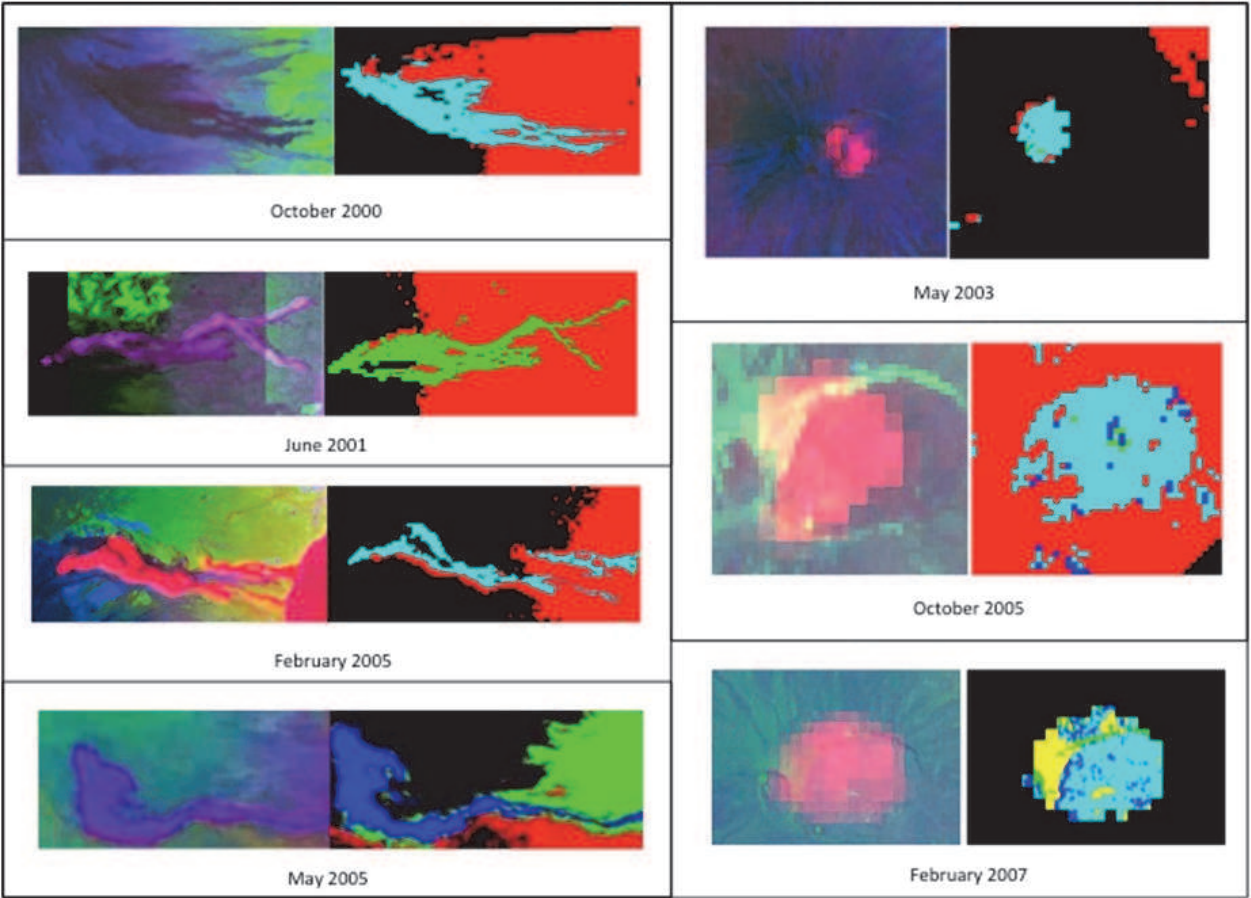

Fig. 8. Automatic extraction of lava flows outlines.

4. Results and interpretations

In order to validate the outlines automatic extraction method, each extraction result has been compared to the referenced outline. The error matrixes (table 4) represent the tests run on the seven tested objects localized on figure 7.

The error matrixes enable calculating global errors of classifications between 77% and 96% (table 4). We can observe a disparity between the summit zone eruptions and those implemented on sloppy substrates with various spectral properties. The first ones show a global precision between 77% and 88%, whereas the others variate from 91% to 96%. This is partly due to low reflectances observed for the substrate at the summit of the volcano. For example, the outlines of a lava flow newly implemented are hardly distinguished from the intra Dolomieu lava effusion zone that presents similar ages. The mean precisions show the same disparity, with values included between 77% and 84% at the summit zone, and included between 86% and 90% for the lava flows situated on the cone's flanks and on the slopes. The area of the lava flows also play a role in the classification precision's difference,

20001012	Lava Flow class	No lava flow class	
Lava Flow Aerial picture	3.422	0.659	4.081
No Lava Flow Aerial picture	0.667	11.602	12.269
Total Area of aerial picture	4.089	12.261	16.35
Global Accuracy		91.89%	
Mean Accuracy		89.205%	
Producer accuracy lava flow		83.85%	
Producer accuracy no lava flow		94.56%	
Mean distance between the outlines		28.41m	
20010611	Lava Flow class	No lava flow class	
Lava Flow Aerial picture	2.620	0.425	3.045
No Lava Flow Aerial picture	0.696	9.039	9.735
Total Area of aerial picture	3.316	9.464	12.78
Global Accuracy		91.228%	
Mean Accuracy		89.445%	
Producer accuracy lava flow		86.04%	
Producer accuracy no lava flow		92.85%	
Mean distance between the outlines		28.54m	
20030530	Lava Flow class	No lava flow class	
Lava Flow Aerial picture	0.2386	0.0445	0.2831
No Lava Flow Aerial picture	0.0784	0.3439	0.4223
Total Area of aerial picture	0.317	0.4223	0.7054
Global Accuracy		82.58%	
Mean Accuracy		82.855%	
Producer accuracy lava flow		84.28%	
Producer accuracy no lava flow		81.43%	
Mean distance between the outlines		30.45m	
20040502	Lava Flow class	No lava flow class	
Lava Flow Aerial picture	1.8389	0.6246	2.4635
No Lava Flow Aerial picture	0.6610	26.2154	26.8319
Total Area of aerial picture	2.4999	26.84	29.2949
Global Accuracy		95.31%	
Mean Accuracy		86.09%	
Producer accuracy lava flow		74.64%	
Producer accuracy no lava flow		97.70%	
Mean distance between the outlines		31.55m	
20050217	Lava Flow class	No lava flow class	
Lava Flow Aerial picture	3.291	0.901	4.192
No Lava Flow Aerial picture	0.816	17.002	17.818
Total Area of aerial picture	4.107	17.903	22.01
Global Accuracy		92.2%	
Mean Accuracy		86.965%	
Producer accuracy lava flow		78.51%	
Producer accuracy no lava flow		95.42%	
Mean distance between the outlines		29.65m	
20051004	Lava Flow class	No lava flow class	
Lava Flow Aerial picture	0.2727	0.0761	0.3488
No Lava Flow Aerial picture	0.1462	1.2272	1.3734
Total Area of aerial picture	0.4189	1.3033	1.7222
Global Accuracy		87.1%	

Automatic Mapping of the Lava Flows at
Piton de la Fournaise Volcano, by Combining Thermal Data in Near and Visible Infrared

215

Mean Accuracy		83.8%	
Producer accuracy lava flow		78.2%	
Producer accuracy no lava flow		89.4%	
Mean distance between the outlines		26m	
20070218	Lava Flow class	No lava flow class	
Lava Flow Aerial picture	0.2960	0.0713	0.3673
No Lava Flow Aerial picture	0.0862	0.2617	0.3479
Total Area of aerial picture	0.3822	0.333	0.7152
Global Accuracy		77.98%	
Mean Accuracy		77.9%	
Producer accuracy lava flow		80.588%	
Producer accuracy no lava flow		75.22%	
Mean distance between the outlines		55.14m	

Table 4. Error matrices for the seven outlines obtained by automatic extraction, by comparing those from the photo-interpretation of aerial photographs with those from automatic extraction.

the summit zone lava flows have less superficy than the ones observed along the slopes. An error on the outline will echo as importantly as the aria of **the mapped** lava flow is low. As to say, the more the mapped lava flow's area is important, the less the error will echo on the precision of the classification. The exactitude of the producer of the "lava flow" class is the most important in the validation of an automatic lava flow outline extraction method. The later varies from 74% and 87% on the entire tested lava flow. There is no observed difference between the eruptions that occur in the Dolomieu crater and the ones that occur on the flanks and the Grandes Pentes of the volcano. On another hand, the morphology of the lava flows plays a role on this precision (figure 8). The more the lava flow's superficy is important and the more compact it is, like a cercle shape form or very large, the more precise the "lava flow" class will be.

The distances between the automatic extracted lava flow outlines, in the case of superimposed lava flows, and those considered as reference is about 30m (table 4 and figure 9). Now, the satellite data used in the automatic extraction have a visible, near and medium infrared spatial resolution from 10m to 20m. If the extraction was realized without any possible confusion, we should have mean distance of about the size of these pixels. Nevertheless, in some low reflectances zones, only the thermal imaging is able to bound the outline's localization zone (figure 8 and 9). It therefore considerably reduces the precision because this data has a 90m pixel. We notice that in zones where the lava regularly effuses, the reflectance's difference cannot allow a free from error extraction of the outline, and it is therefore deducted from the thermal mask. This mask is essential because it allows the definition of a zone of interest inside witch the outline can be determined. There is no possible confusion: to one thermal data, only one lava flow can be associated.

In vegetalized zones, the extraction can be considered as a simple threshold of the infrared, the outline is then about the size of the pixel. In some zones, especially the Dolomieu crater or certain parts of the cone, the differences of reflectances of the lava flows don't allow to differentiate them. The outline is then obtained thanks to the thermal data. It can represent up to 40% of the summit zone lava flows outline, but only 5% to 0% of the proximal and distal eruption's outlines. The mean error observed on the outline's extraction can then reach twice the size of the optical data's pixel. Some light diffusion and wedging effects can interact on the precision.
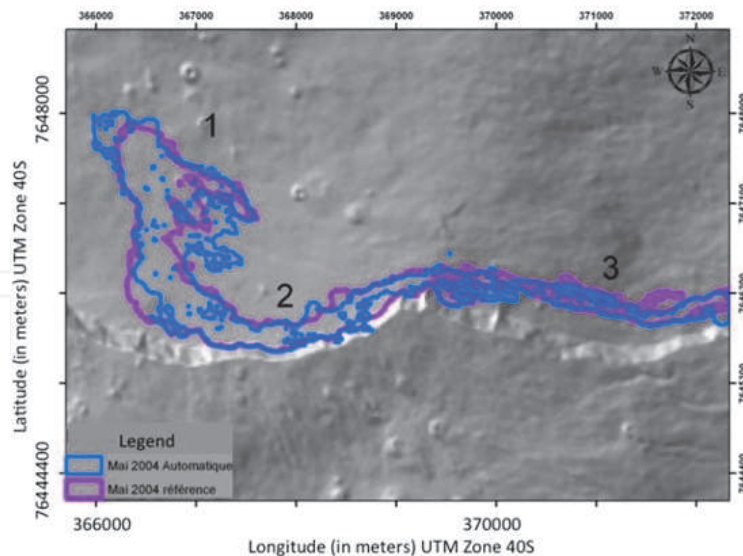
Fig. 9. Automatic lava flow outline extraction of May 2004 (blue) compared with the referenced outline (purple).

Lets consider the example of the May 2004 lava flow (figure 9 and table 4). Three zones are sharply distinguished in the extraction: a very low reflectance and high thermal zone (1), a low reflectance with few or no thermal diffusion zone (2), and a various reflectance with few or no thermal diffusion zone (3). The weakest precision is for the first zone, for the second zone, the low reflectance is due to the substrate's nature and to luminosity issues in the zone, because the shadow projected by the rampart can interfere. A luminosity parameter is to be taken into consideration when choosing and time acquiring SPOT data. As for the extraction of the third zone, the thermal infrared band essentially obtains it, because the lava flow implemented in a vegetalized zone with a high spectral signature difference compared to the lava flow. It is the zone where the extraction is the most precise because only based on the SPOT data.

5. Discussion and conclusion

The vectors of the outlines obtained by automatic extraction properly match with the referenced outlines since we obtain a mean exactitude producer of 80% for the "lava flow" class. If we compare our automatic extraction results to those obtained by DGPS, they are less precise. The DGPS has a precision of about one centimeter at its antenna, now it's the operator who transports it. The error is due to the positioning of the antenna regards to the outlines. The error then is about one meter, for pluri-meter in our extractions. Nevertheless, the effusion zones are not all accessible, and cannot let realizing the outlines in their integrality, especially in the Grandes Pentes. Computer assisted drawing methods are on the other hand less reliable than our methodology for the data' distortion are not taken into account and can provoke hundred of meters error. The results of our classification are close to those obtained in other contexts' literature. (Azerzaq et al., 1997 ; Messar et Messar, 1997 ; Yüksel et al., 2008).

The vectorization time by photo-interpretation can take several days, whereas the automatic method enables obtaining this vector in less than one hour. There is therefore a considerable

gain of time. The gaps of observations due to clouds, or zone with high thermal diffusion and low reflectances, could be filled by using RADAR imaging in treatment sequences (Weisseil et al.2004). However, by adding Bi data will increase the treatment time, especially by using coherence data.

The association of thermal and optical data has already been realized in other automatic classifications with outlines extractions contexts: glaciology (Raciviteanu et al. 2008), the canopy (Joshi et al., 2006), agriculture (Kasdan, 1979; Saito et al., 2001). For similar spectral resolution data, the error matrix results are comparable to those obtained by our methodology.

This methodology was developed in order to automate lava flow outline's extraction and therefore ensure a fast update of the Piton de la Fournaise's database. The lava flow map was updated thanks to photo-interpretation and automatic extraction (figure 4). It allowed us to test the reliability of the outlines extracted according to each methodology used in this article, and to know their precision.

The errors measured by the matrixes give us the extracted surface's error, by comparing the automatic lava flow's area and the referenced one. We saw that: 1/ the difference of interpretation between two operators for the same data can be of 2% for the aerial photos and it varies between 2% and 5% with satellite data. 2/if the outlines extracted from satellite data's photo interpretation are compared to those extracted from aerial data, the exactitude producer of the "lava flow" class can reduce to 80%, but is at an average of 90%. 3/ Those obtained with the same type of data varies from 74% to 87%, which is to say an average of less than 10%. It influences the obtained area in less than 10%, exception made for low scale summit zone eruptions which represent an error of 20%, which remains modest and without major consequences on the volume and production estimation rates for the volcano.

6. Acknowledgements

7. Note

All the lava flow outlines' vectors will be available online on the Laboratoire de Geosciences Reunion website.

8. References

Abrams M., Abbott E., KahleA., 1991. Combined Use of Visible, Reflected Infrared, and Thermal Infrared Images for Mapping Hawaiian Lava Flows. Journal of Geophysical Research, n°96 (B1), pp. 475-484.

Azerzaq M., Assafi M., Fahsi A., 1997. Utilisation des images HRV de SPOT pour la détection du changement périurbain à Casablanca (Maroc). Télédétection des milieux urbains et périurbains. Éd. AUPELF-UREF, pp. 275-282.

Bachèlery P., 1981. Le Piton de la Fournaise (Ile de la Réunion). Étude volcanologique, structurale et pétrologique. Thesis manuscript, Univ. Clermont-Ferrand II, 1-215.

Billard G., 1974. Carte Géologique de l'île de la Réunion. 1 :50000.Bureau de Recherche Géologique et Minières, Paris. pp. 1-4.

Bonneville A., Lanquette A.M., Pejoux R.1989. Reconnaissance des principales unités géologiques du Piton de la Fournaise, La Réunion, à partir de SPOT 1. Bulletin de la société géologique de France, n°87, pp. 1101-1110.

Bussière P., 1967. Carte Géologique du département de La Réunion, 1 :1000000. Service de la Carte Géologique de la France.

Courtillot V., Besse J., Vandamme D., Montigny R., Jaeger J-J., Cappetta, H., 1986. Deccan flood basalts at the Cretaceous/Tertiary boundary? Earth and Planetary Sciences Letters, n°80 (3-4) , pp. 361-374.

De Michele M., Briole P., 2007. Deformation between 1989 and 1997 at Piton de la Fournaise volcano retrieved from correlation of panchromatic airborne images. Geophysical Journal International, n°169, pp. 357–364.

Despinoy M., 2000. Potentiel de la télédétection haute résolution spatiale et spectrale en milieu intertropical. Une approche transdisciplinaire à partir d'expériences aéroportées à la Réunion et en Guyane française. Thesis manuscript, pp.1-244.

Favalli M., Karátson D., Mazzarini F., Pareschi M.T., Boschi E., 2009, Morphometry of scoria cones located on a volcano flank: A case study from Mt. Etna (Italy), based on high-resolution LiDAR data. Journal of Volcanology and Geothermal Research, v. 186, p. 320-330.

Froger J.-L., Fukushima Y., Tinard P., Cayol V., Souriot T., Mora O., Staudacher T., Durand Ph., Fruneau B., Villeneuve N.,2007. Multi Sensors InSAR Monitoring of Volcanic Activity: The February & April 2007 Eruptions at Piton de la Fournaise, Reunion Island, Imaged with ENVISAT-ASAR and ALOS-PALSAR data. Proc. of FRINGE 2007 Workshop, Frascati, Italy,

Habib T., Chanussot J., Inglada J., Mercier G., 2007. Abrupt change detection on multitemporal remote sensing images: a statistical overview of methodologies applied on real cases. Proceedings IEEE IGARSS, pp. 2593–2596.

Harris A.J.L., Dehn J., James M.R., Hamilton C., Herd R., Lodato L., Steffke A., 2007, Pahoehoe flow cooling, discharge, and coverage rates from thermal image chronometry. Geophysical Research Letters, n° 34, pp. 6.

Hirn B.R., Di Bartola C., Ferrucci F.,2005. Automated, Multi-Payload, High-Resolution Temperature Mapping and Instant Lava Effusion Rate Determination at Erupting Volcanoes. Geoscience and Remote Sensing Symposium, 2005. IGARSS '05. Proceedings. IEEE International. n° 7, pp. 5056 – 5059.

Honda K., Nagai M., 2002. Real-time volcano activity mapping using ground-based digital imagery. ISPRS Journal of Photogrammetry and Remote Sensing, n°57(1-2), pp.159-168.

Inglada J., Favard J-C., Yesou H., Clandillon S., Bestault C., 2003. Lava flow mapping during the Nyiragongo January, 2002 eruption over the city of Goma (D.R. Congo) in the frame of the international charter space and major disasters. Proceedings of

the IEEE International Geoscience and Remote Sensing Symposium, IGARSS '03, n°3, pp.1540- 1542.

James M.R., Pinkerton,H., Robson S., 2007, Image-based measurement of flux variation in distal regions of active lava flows. Geochem. Geophys. Geosyst., n° 8, pp. Q03006.

Joshi C., De Leeuw J., Skidmore,A.K., Van Dure, I.C., Van Oosten, H., 2006. Remotely sensed estimation of forest canopy density: a comparison of the performance of four methods. International Journal of Applied Earth Obeservation and Géoinformation. n°8, pp.84-95.

Kahle A.B., Abrams M.J., Abbott E.A., Mouginis-Mark P.J., Realmuto V.J., 1995. Remote sensing of Mauna Loa. Mauna Loa Revealed: Structure, Composition, History, and Hazards. Geophys. Monogr. N°92, AGU, pp. 145–169.

Kahle A., Gillespie A., Abbott E., Abrams M, Walker R., Hoover G., Lockwood J.P., 1988. Mapping and relative dating of Hawaiian basalt flows using multispectral thermal infrared images. Journal of Geophysical Research, n°93(B12), pp. 239-251

Kasdan H., 1979. Feasibility of Using Optical Power Spectrum Analysis Techniques for Automatic Feature Classification from High Resolution Thermal, Radar, and Panchromatic Imagery. Recognition systems inc van nuys calif, pp. 1-194

Lacroix A., 1936. Le volcan actif de l'île de la Réunion et ses Produits. Paris, Gauthier et Villard ed., pp. 1-297

Legelay-Padovani A., Mering C., Guillande R., Huaman D., 1997. Mapping of lava flows through SPOT images - an example of the Sabancaya volcano (Peru), International Journal Remote Sensing, n°18(15), pp. 3111-3133.

Lénat J.-F., 1987. Structure et Dynamique internes d'un volcan basaltique intraplaque océanique : le Piton de la Fournaise (Ile de la Réunion). Thèse de doctorat d'Etat, Univ. Clermont II, France.

Lénat J.F., Bachèlery P. ,1987. Dynamics of Magma Transfer at Piton de La Fournaise Volcano (Réunion Island, Indian Ocean), Earth Evolution Sciences, Special Issue "Modeling of Volcanic Processes", Chi-Yu and Scarpa (Eds.), pp. 57-72, Friedr. Vieweg and Sohn, Brauschweig/Wiesbaden

Lénat J.-F., Bachèlery P. et Desmulier F., 2001 . Genèse du champ de lave de l'Enclos Fouqué : une éruption d'envergure exceptionnelle du Piton de la Fournaise (Réunion) au 18 ème siècle. Bull. Soc. Géol Fr. 2, pp.177-188.

Letourneur L., Peltier A., Staudacher T., Gudmundsson A., 2008, The effects of rock heterogeneities on dyke paths and asymmetric ground deformation: The example of Piton de la Fournaise (Réunion Island). Journal of Volcanology and Geothermal Research, n°173, pp. 289-302.

Lombardo V., Harris A.J.L., Calvari S., Buongiorno M.F., 2009, Spatial variations in lava flow field thermal structure and effusion rate derived from very high spatial resolution hyperspectral (MIVIS) data. Journal of Geophysical Research, n° 114, pp. B02208.

Lu Z., Rykhus R., Masterlark T., Dean K.G., 2004, Mapping recent lava flows at Westdahl Volcano, Alaska, using radar and optical satellite imagery. Remote Sensing of Environment, n°91(3-4), pp. 345-353.

Messar Y., Messar N., 1997. Apport de la télédétection à la cartographie de l'espace urbain au 1: 20000 en terme d'emprise au sol du bâti : cas de la ville d'Oran (Algérie). Télédétection des milieux urbains et périurbains. Éd. AUPELF-UREF., pp. 315-323.

Observatoire Volcanologique du Piton de La Fournaise internal annual report, 2009

Observatoire Volcanologique du Piton de La Fournaise internal report, janvier 2010

Paparoditis N., Souchon J-P., Martinoty G., Pierrot-Deseilligny M., 2006. High-end aerial digital cameras and their impact on the automation and quality of the production workflow. ISPRS Journal of Photogrammetry & Remote Sensing, n°60, pp. 400–412.

Peltier A., Bachèlery P., Staudacher T., 2009. Magma transport and storage at Piton de la Fournaise (La Réunion) between 1972 and 2007: A review of geophysical and geochemical data. Journal of Volcanology and Geothermal Research, n°184, pp. 93-108.

Raciviteanu A.E., Williams M.W., Barry R.G., 2008. Optical Remote Sensing of Glacier Characteristics: A Review with Focus on the Himalaya. Sensors , n°8, pp. 3355-3383

Saito G., Ishitsuka N., Matano Y., Kato M., 2001. Application on Terra/ASTER data on agriculture land mapping. Paper presented at the 22nd Asian Conference on Remote Sensing, Singapore, pp.1-6

Servadio Z., Villeneuve N., Gladys A., Staudacher T., Urai M., 2008. Preliminary results of lava flow mapping using remote sensing in Piton de la Fournaise, La Réunion island. Workshop on the "Use of Remote Sensing Techniques for Monitoring Volcanoes and Seismogenic Areas", IEEE Naples. Poster session and Proceeding.

Stieltjes L., Moutou P., 1989. A statistical and Probabilitic study of the historic activity of Piton de la Fournaise, Reunion Island, Indian Ocean. Journal of Volcanology and Geothermal Research, n°36, pp. 67-86.

Tinard P., 2007. Caractérisation et modélisation des déplacements du sol associés à l'activité volcanique du Piton de la Fournaise, île de La Réunion, à partir de données interférométriques. Août 2003 – Avril 2007. Ph.D. Thesis, Univ. Blaise Pascal, pp.1-334

Villeneuve N., 2000. Apports multi-sources à une meilleure compréhension de la mise en place des coulées de lave et des risques associés au Piton de la Fournaise : Géomorphologie quantitative en terrain volcanique. Thesis manuscript, pp.1-378.

Villeneuve N., Bachèlery P., 2006. Revue de la typologie des éruptions au Piton de La Fournaise, processus et risques volcaniques associés. Cybergéo : revue européenne de Géographie, n° 336

Yüksel A., Akay A.E., Gundogan R., 2008. Using ASTER Imagery in Land Use/cover classification of Eastern Mediterranean Landscapes According to CORINE Land Cover Project. Sensors. n° 8,pp. 1237-1251.
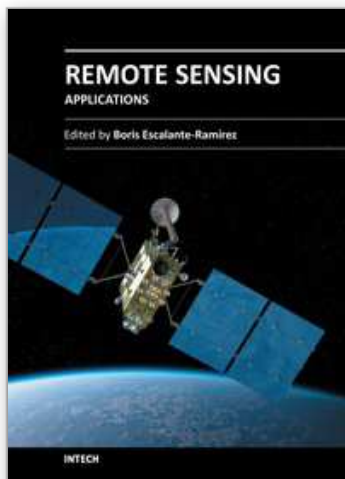
Remote Sensing - Applications

Edited by Dr. Boris Escalante

Nowadays it is hard to find areas of human activity and development that have not profited from or contributed to remote sensing. Natural, physical and social activities find in remote sensing a common ground for interaction and development. This book intends to show the reader how remote sensing impacts other areas of science, technology, and human activity, by displaying a selected number of high quality contributions dealing with different remote sensing applications.

How to reference

In order to correctly reference this scholarly work, feel free to copy and paste the following:

Z. Servadio, N. Villeneuve and P. Bachèlery (2012). Automatic Mapping of the Lava Flows at Piton de la Fournaise Volcano, by Combining Thermal Data in Near and Visible Infrared, Remote Sensing - Applications, Dr. Boris Escalante (Ed.), ISBN: 978-953-51-0651-7, InTech, Available from: http://www.intechopen.com/books/remote-sensing-applications/automatic-mapping-of-the-lava-flows-at-piton-de-la-fournaise-volcano-by-combining-thermal-data-i

INTECH
open science | open minds